Simulation and POD analysis of the flow field in a reach of the Hudson River Estuary

N.M. T. Phan & J.C. Wells
Ritsumeikan University, Shiga, Japan

W. D. Kirkey, M.S. Islam, C. B. Fuller, T.O. Ojo & J.S. Bonner
Clarkson University, New York, USA

ABSTRACT: We present high-resolution large-eddy simulation of the flow in a bend of the Hudson River (New York, USA) around the West Point using Fluent 13.0.0. Near-bank resolution is set to some 2 meters in order to resolve large-scale turbulent motions in the near-bank regions. The simulation is performed at a constant discharge corresponding to a typical ebb tide, with neglect of buoyancy. To validate our simulation, field measurements of discharge and velocity in a reach around West Point are performed. Proper Orthogonal Decomposition (POD) is used to extract coherent structures from simulation results. POD modes are orthogonal flow fields that capture the kinetic energy in an optimally convergent fashion. Results show that only a few low-order POD modes suffice to describe the most energetic motions in the flow.

1 INTRODUCTION

Large-scale turbulent structures contain most of the turbulent kinetic energy of the flow. In regions with abrupt changes in geometry such as bends or confluences, flow separation occurs and large-scale turbulent structures develop. Turbulence and its fluctuation contribute to the transport of mass, momentum and energy. The proper understanding and prediction of the flow and turbulence characteristics is thus of importance in river engineering.

With the rapid increase in computer power during the past few decades, three-dimensional numerical approaches of river flows are becoming feasible tools for investigating the flow structures. Several 3D Reynolds Averaged Navier-Stokes (RANS) models have been carried out for river calculations (Shimizu et al. 1990; Sinha et al. 1998; Hodskinson & Ferguson 1998; Lane et al. 1999; Ma et al. 2002; Rodriguez et al. 2004). In this approach, mean-flow quantities are solved by Reynolds averaged equations and turbulence effect are modeled by a RANS turbulence model. The works in literature showed that the RANS turbulence models only capture effectively mean flow characteristics in rivers. Large-Eddy Simulation (LES), on the other hand, allows unsteady solutions that resolve large-scale turbulent eddies. As LES calculations are expensive, there have been some attempts in applying the LES to river-related flows (Bradbrook et al. 2000; Van Balen et al. 2010; Kang et al. 2011). Bradbrook et al. (2000) performed LES to investigate periodic flows in a natural river confluence. Van Balen el al. (2010) used LES to study a curved open-channel flow over topography, and showed a qualitative agreement between the LES and experimental results. In particular, the LES results in their work reveal a recirculation zone near the inner bend and a mixing layer as well as strong upwelling flow motion at the interface between the recirculation zone and the main flow. Especially, Kang et al. (2011) performed high-resolution computations for a flow in a small outdoor channel with complex bathymetry, using both unsteady RANS models and LES, and showed the advantage of the LES in prediction of the existence of a sharp shear layer emanating from the inner bank and spreading toward the outer bend. Therefore, the LES is promising but its application to natural rivers still remains a challenge (Rodi 2010).

Some works were done in comparison between Acoustic Doppler Current Profiler (ADCP) measurements and computations in a river (Baranya & Jozsa 2006) and an estuary (Stacey et al. 1999). Baranya & Jozsa (2006) compared velocity profiles measured by the boat-mounted ADCP and those modeled by the k-ε model in a CFD code in a meandering reach of Danube River. Stacey et al. (1999) used a four-beam broadband ADCP to directly measure Reynolds stress profiles, which are based on along-beam velocities, in northern San Francisco Bay. The dataset was compared with the popular Mellor-Yamada 2.5 closure. In the knowledge of the author, there have been no reports to compare measured turbulence properties by Horizontal

Acoustic Doppler Current Profiler (HADCP) with the LES at river banks.

The Hudson River (New York, USA) originates northwest of Albany and extends nearly 600 km to New York City. The Lower Hudson River, approximately 250 km long from the Federal Dam at Troy to the Battery at the southern tip of Manhattan Island, is a tidal estuary. Depending on river discharge conditions, salinity intrusion extends from 30 to 100 km north of the Battery. The freshwater inflow at the Federal Dam ranges from 100 m^3/s in summer to the order of 2000 m^3/s in spring. Typical tidal range is 1.5 m, and the tidal velocities can reach 1 m/s during springtides.

There have been some numerical simulations of the Hudson River (Warner et al. 2005; Blumberg & Mellor 1987). Warner et al. (2005) used a three-dimensional Regional Ocean Modeling System (ROMS) model with turbulence closure methods of k-ε, k-ω, and k-kl to predict the velocity and salt transport. Blumberg & Mellor (1987) proposed Estuarine, Coastal and Ocean Model (ECOM), a derivative of the Princeton Ocean Model (POM) to model the Hudson River. The results of this model are displayed on the New York Habor Observing and Prediction System (NYHOPS). These models applied RANS method. The resolution in their models is about 100 m in the horizontal and 10-20 points in the vertical. This resolution captures the overall hydrodynamics well, but may not suffice to capture large scale turbulent motions in near-bank regions, especially near river bends or embayments.

We here present high-resolution 3D simulation of a flow in a small bend of the Hudson River around West Point HADCP location (Fig. 1a) using Fluent 13.0.0. The bathymetry of this reach is complex, with a large change in depth in mid-channel (Fig. 1b). Large-aspect-ratio elements appear at shallow regions near the bank. Therefore, the meshing for this reach is not easy. Moreover, we concentrate on simulating the flow field at a constant discharge corresponding to a typical ebb tide. The standard Smagorinsky turbulence model and Werner and Wengle's wall model for the smooth wall are used with assumption of no buoyancy.

To analyze the flow field, we apply Proper Orthogonal Decomposition (POD). This method, which is similar to Fourier decomposition, has been used in many applications such as image processing (Sirovich & Kirby 1987), and derivation of reduced-order dynamical models (Holmes et al. 1998). Besides, POD analysis was applied to optimize locations for sensor placement and accurate reconstruction of velocity, salinity and temperature in the ocean (Yildirim et al. 2009). Another work is the development of a "virtual" nowcasting system based on the POD technique for real-time estimation of contaminant dispersion to the unsteady flow past a surface-

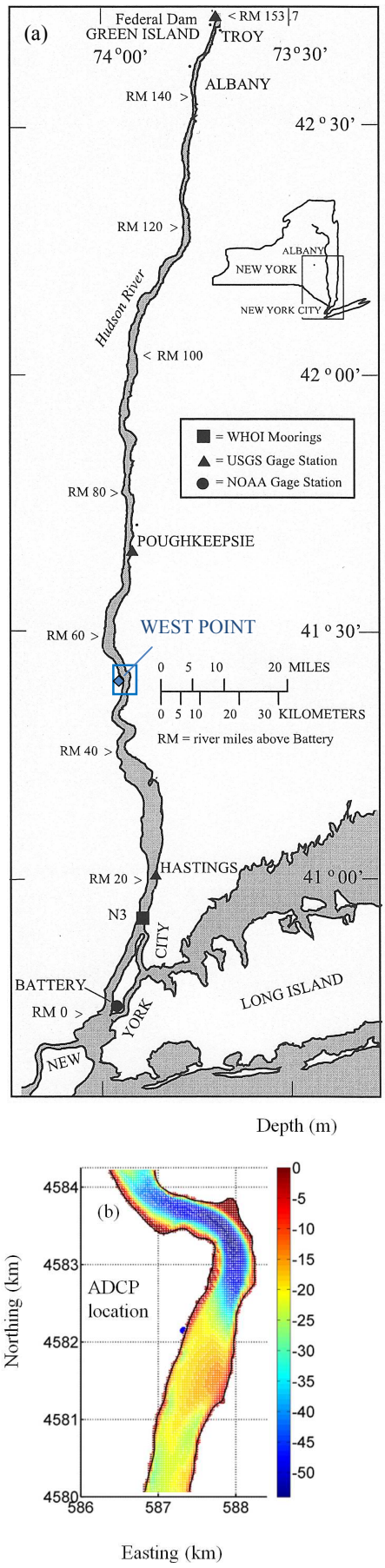

Figure 1. (a) The Lower Hudson River (Warner et al. 2005) with permission). (b) The location and bed elevation of a reach around West Point HADCP location

mounted cube, which is chosen as a prototype for the wind environment in a city (Mokhasi et al. 2009).

The outline of this paper is as follows. The LES method and POD are first described. This is followed by a comparison of the simulation results with ADCP data. The application of POD to the simulation results is then presented. Finally, we give some comments and discuss future work.

2 NUMERICAL METHODS

The governing equations in Large Eddy Simulation of river flows are the spatially-filtered three-dimensional incompressible continuity and Navier-Stokes equations. The filter width is determined by the grid spacing. Small-scale motions of turbulence cannot be resolved on a given grid, so their effect is represented by the sub-grid-scale (SGS) stresses appearing in the filtered equations of momentum, which are modeled. The most commonly used model is based on eddy-viscosity μ_t:

$$\tau_{ij} - \frac{1}{3}\tau_{kk}\delta_{ij} = -2\mu_t \overline{S_{ij}} \tag{1}$$

where the overbar denotes the grid filtering operation and S_{ij} is the strain rate tensor. The eddy-viscosity-based model used here is the standard Smagorinsky model in which the sub-grid turbulence viscosity is modeled using a mixing-length relationship:

$$\mu_t = \rho L_s{}^2 \left|\overline{S}\right| \tag{2}$$

where L_s is the mixing length of sub-grid scales and $\left|\overline{S}\right|$ is the magnitude of the strain rate tensor S_{ij}. In the finite-volume method, L_s is determined by

$$L_S = \min\left(\kappa d, C_S V^{1/3}\right) \tag{3}$$

where κ is the von Karman constant, d is the distance to the closest wall, C_s is the Smagorinsky constant ($C_s = 1$), and V is the volume of the computational cell.

3 COMPUTATIONAL SETUP

The bathymetric data was produced from a combination of National Oceanic and Atmospheric Administration (NOAA) and SUNY Stony Brook datasets. Bathymetry data is gridded by 30x30 m resolution in the North American Datum of 1983 using the Universal Transverse Mercator coordinate system. The pre-processor Gambit® is employed for mesh generation. With a length of 5000 m, width of 700 m, and maximum depth of 54 m, the horizontal grid spacing is 2 – 20 m and 20 layers in depth which are finer near the bed.

We perform the LES simulation of the river reach corresponding to ebb tide, but at constant discharge $Q = 7120$ m^3/s. The surface water level is taken to be zero in NAVD88 datum. The mean water depth H is 20 m and the average velocity is 0.57 m/s. The Reynolds number based on this velocity and the mean water depth is 11×10^6. Furthermore, buoyancy effects are neglected.

The commercial software package Fluent 13.0.0 is used. The principle method in Fluent is a finite-volume method, converting governing equations into algebraic equations on control volumes that can be solved numerically. For low speed incompressible flows, pressure-based approach is chosen. In this method, the velocity is obtained from the momentum equations and the pressure is obtained by solving the Poisson equation. Coupling of the pressure and momentum equations is achieved using the SIMPLE algorithm. The temporal integration is carried out by an implicit scheme with second-order accuracy. The spatial derivatives are approximated by second-order central difference. The computational time step is 2 seconds for the unsteady solution. All unsteady simulations are started from a converged solution of steady RANS using the standard k–ε model.

Werner and Wengle's near-wall treatment based on power-law profiles for the near-wall velocity outside the viscous sublayer is used in LES to account for the boundary layer formation at the far field regions where the mesh is coarser. However, this wall model is not for rough walls while the log-law for the rough walls can be applied in RANS. Roughness k_s is set as 0.002 m (Warner et al. 2005)

The boundary condition at the bed and the bank of the reach is the non-slip boundary condition. At the inlet, the log law velocity profile is applied. The turbulence inflow conditions are specified by turbulence intensity of 10% and turbulence viscosity ratio of 10. At the outlet, zero gradient boundary conditions are employed. At the surface, a free-slip boundary condition is applied.

4 PROPER ORTHOGONAL DECOMPOSITION

The POD was proposed as a means for defining coherent structures in turbulent flows (Lumley 1967). The truncated (N ≠ ∞) POD approximation to a velocity field $\mathbf{u}(\mathbf{x},t)$ is given by

$$\mathbf{u}(\mathbf{x},t) \cong \sum_{k=1}^{N} \zeta_k(t)\boldsymbol{\psi}_k(\mathbf{x}) \tag{4}$$

where $\zeta_k(t)$ are called the temporal coefficients, and $\boldsymbol{\psi}_k(\mathbf{x})$ are orthogonal spatial basis functions which are the eigenfunctions of the two-point correlation tensor $\mathbf{R}(\mathbf{x},\mathbf{x}')$ defined as

$$\mathbf{R}(\mathbf{x},\mathbf{x}') = \lim_{T\to\infty} \frac{1}{T} \int \mathbf{u}(\mathbf{x},t)\mathbf{u}(\mathbf{x}',t)dt \tag{5}$$

i.e. the basis functions are solutions to the Fredholm integral equation

$$\int_D \mathbf{R}(\mathbf{x},\mathbf{x}') \cdot \boldsymbol{\psi}(\mathbf{x}')d\mathbf{x}' = \lambda\boldsymbol{\psi}(\mathbf{x}) \tag{6}$$

Thus, it may be shown that they are statistically optimal in that their energy converges faster than any

other set of functions in Hilbert space ((Holmes et al. 1998). The eigenvalues λ represent the kinetic energy of the flow in each POD mode. The POD decomposition is a spectral decomposition in which the eigenfunctions and eigenvalues are sorted in order of decreasing eigenvalue.

The decomposition also satisfies the orthogonality properties

$$\int_D \boldsymbol{\psi}_i(\mathbf{x}) \cdot \boldsymbol{\psi}_j(\mathbf{x}) d\mathbf{x} = \delta_{ij} \tag{7}$$

$$\lim_{T\to\infty} \frac{1}{T} \int_0^T \zeta_i(t)\zeta_j(t) dt = \lambda_i \delta_{ij} \tag{8}$$

Analagous relations hold for the discretized version of POD that, in practice, is computed from a finite time series of flow snapshots.

5 RESULTS AND DISCUSSION

5.1 *Simulation vs. ADCP Data*

A 600kHz Horizontal ADCP manufactured by Teledyne RD Instruments Inc. is installed on a pier near the USGS gauging station at West Point. This location is about 20 m far from the western bank of the Hudson River. The HADCP measures the velocity on a horizontal transect of the river at the approximate depth of 3 – 4 m from the river bed with a resolution in time of 1 minute. Figure 2 shows time series of 30-minute averages of HADCP velocity on October 25th, 2011 at three horizontal locations with distances d = 5 m, 15 m and 80 m from the location of HADCP sensor. Vectors represent flow direction in time. The water flows south during ebb tide. Velocities during flood tide is much smaller than those during ebb tide at d = 5 m. It may be due to the north-south asymmetry in bathymetry around the HADCP location. In ebb tide, high-speed water comes from the deep main channel and spreading spanwise. In flood tide, the upstream flow region (to the south) is much shallower. We also made discharge measurements near the HADCP location using a downward-looking bottom-tracking ADCP mounted on a boat on this day. The discharge is shown in Figure 3.

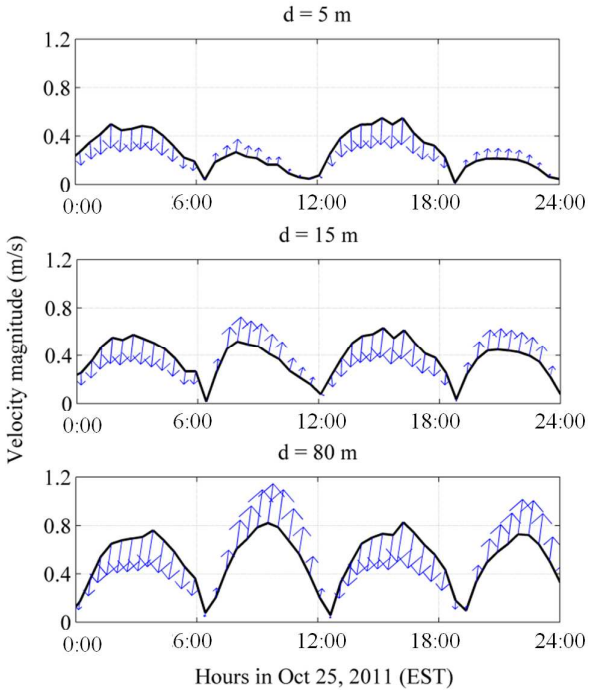

Figure 2. Time series of HADCP velocity on Oct 25th 2011 at horizontal distances d = 5, 15 and 80 m from the location of HADCP West Point. Curves show amplitude, vectors show flow direction. The data are 30-minute averages.

Figure 4 shows time-averaged velocities from URANS k–ω SST model, which was used in Kang et al. (2010), and LES with the corresponding root-mean-square velocities at some distances d from the location of HADCP sensor. The "r.m.s. crosses" is at the heads of the vectors, and the tail at the measurement points. The computational data is in compari-

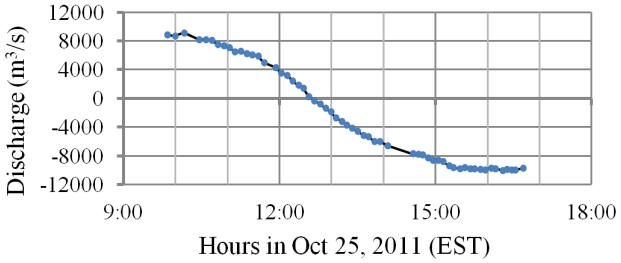

Figure 3. Discharge measured by boat-mounted ADCP on Oct 25th, 2011.

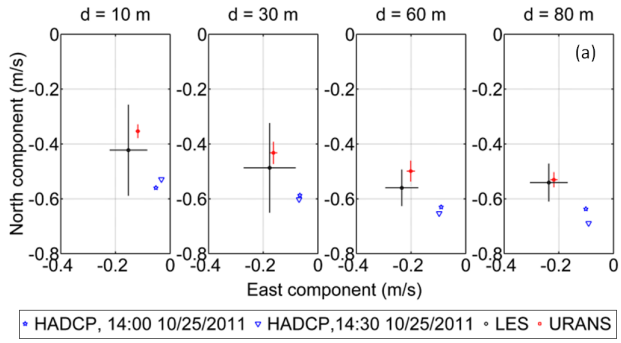

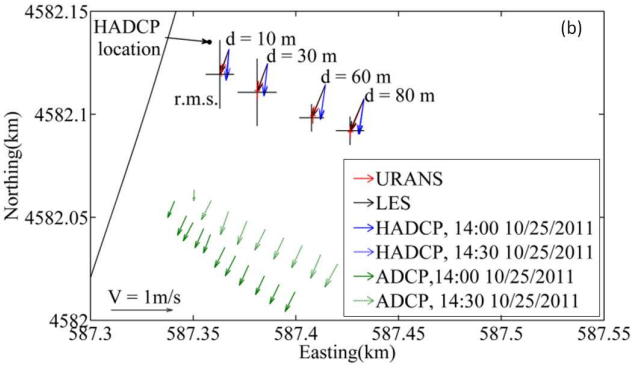

Figure 4. (a) Time-averaged velocities and r.m.s velocities obtained from LES and URANS k-ω SST model compared with 1-minute average of HADCP velocities and (b) depth-average velocities from a boat-mounted ADCP at 14:00 Oct 25, 2011 (Q = 6550 m3/s) and 14:30 Oct 25, 2011 (Q = 7700 m3/s). d is horizontal distance from the location of HADCP sensor at West Point.

son with one-minute average of HADCP velocities and depth-averaged velocities from a boat-mounted ADCP downstream of HADCP location at 14:00 and 14:30 Oct 25th, 2011. We here ran URANS and LES with the same grid and flow condition Q = 7120 m^3/s. For comparison, discharge measured at 14:00 and 14:30 Oct 25th, 2011 is 6550 and 7700 m^3/s. Computations yield lower velocities than HADCP data. The time-averaged velocity obtained from the LES is larger than those from the URANS. It may be because of roughness effect was taken into account in RANS. The LES gives more r.m.s. velocity fluctuation in time near the bank. The flow direction measured from HADCP is different with computational data and boat-mounted ADCP data.

5.2 *POD analysis*

POD analysis is used to extract statistically dominant patterns of velocity at the surface from LES results. Figures 5-7 show results of the surface velocity POD decomposition from 73 LES snapshots sampled at 10 minute intervals. The energy spectrum and cumu-

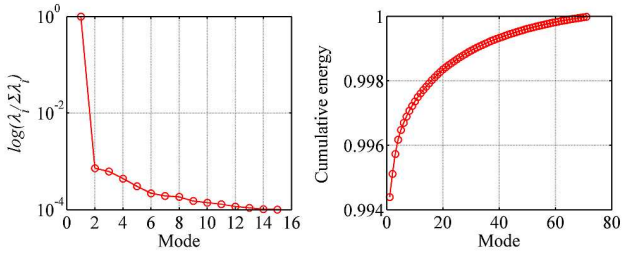

Figure 5. (a) Energy spectra of the first 15 POD modes and (b) cumulative energy from POD decomposition of 73 LES snapshots of surface velocity

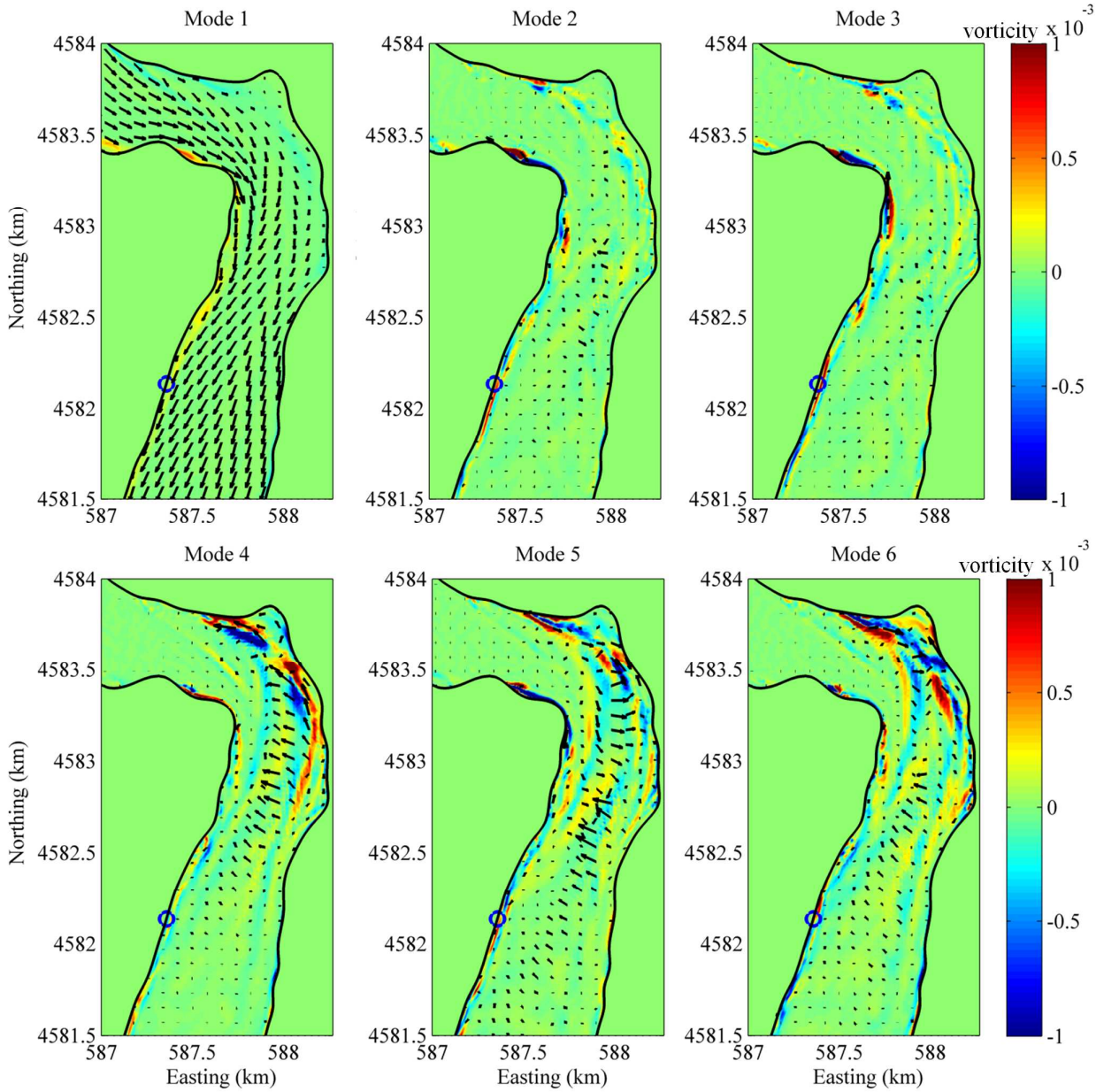

Figure 6. Low-order POD velocity modes. Color is corresponding vorticity of POD modes. Circle is the location of HADCP.

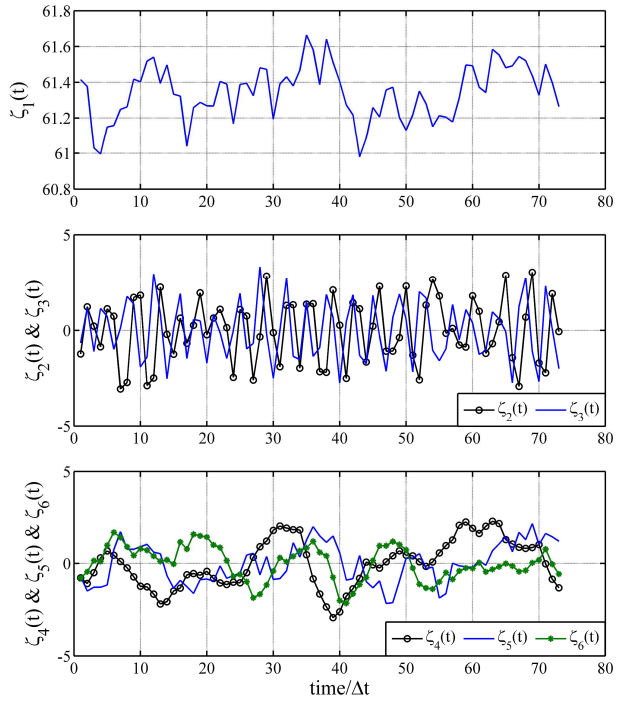

Figure 7. POD coefficients. Solid line is odd coefficients.

lative energy of the POD modes are shown in Figure 5. The eigenvalues are equivalent to the amount of energy that is captured in each mode, and the sum of the eigenvalues equals the total energy. Energy contained in mode 1 is found to contribute more than 99.4% of the total energy of the flow at the surface. This energy captured is very high as turbulence at the surface is rather weak. The POD basis function of mode 1 closely approximates the mean flow.The first 6 POD basis functions and their corresponding vorticity are shown in Figure 6, and the time evolution of the POD coefficients of these modes is shown in Figure 7. In mode 2 and 3, vortices occur briefly near the bank, particular the western bank where the HADCP is installed. Meanwhile, modes 4-6 show vortices emanating from the outer bank to the inner bank downstream of the bend. It can be seen that the temporal POD coefficients of mode 2 and 3 fluctuate more rapidly than POD coefficients of modes 4-6. The low-order modes shown in Figure 6 can reveal statistically dominant structures at the surface, which capture most of the energy of the surface flow there (99.7%). If the flow in rivers or oceans is found to be low-dimensional, only a few modes can reproduce the essential dynamics (Yildirim et al. 2009).

6 CONCLUSION

The LES simulation is compared with the URANS k-ω SST model and ADCP data at West Point. Generally, the computational data match with measurement data in velocity magnitude. The flow direction measured from HADCP is found not parallel to boat-mounted ADCP data. LES gives more fluctuation than RANS near the bank. Until now, a rough wall model has been applied in RANS, not in LES.

Proper Orthogonal Decomposition is applied for 73 LES snapshots of surface velocity. The POD analysis has been very effective to identify coherent structures in turbulent flows (Lumley 1967). In addition to vortices near the bank in mode 2 and 3, vortices emerge from the outer bank and spread to the inner bank downstream, as shown in modes 4-6. The POD results also show that only a few low-order POD modes capture the large energy content of the surface flow. This suggests that these modes can be used to describe dynamics in complex, multi-scale flow in rivers, estuaries and oceans (Yildirim et al. 2009). We hope that real-time prediction of 3D turbulent flow field can be done by tracking the evolution of POD coefficients for a long time using Kalman filter (Frolov et al. 2009). Accordingly, both the data assimilation problem and the forecasting problem can be re-formulated using the POD modes.

In the future work, we will do LES simulation for the flood tide using Fluent. We will also perform ROMS, a popular model based RANS for tidal flow, in a larger domain to provide a 3D overview of the flow field in the Hudson River, as well as support for the LES simulation.

7 REFERENCES

Van Balen, W., Uijttewaal, W.S.J. & Blanckaert, K. 2010. Large-eddy simulation of a curved open-channel flow over topography. *Physics of Fluids* 22(7): 075108.

Baranya, S. & Jozsa, J. 2006. Flow analysis in river Danube by field measurement and 3D CFD turbulence modelling. *Periodica Polytechnica, Civil Engineering* 50(1): 57–68.

Blumberg, A.F. & Mellor, G.L. 1987. A description of a three-dimensional coastal ocean circulation model. *Three-dimensional coastal ocean models* 4: 1–16.

Bradbrook, K.F., Lane, S.N., Richards, K.S., Biron, P.M. & Roy, A.G. 2000. Large Eddy Simulation of periodic flow characteristics at river channel confluences. *Journal of Hydraulic Research* 38(3): 207.

Frolov, S., Baptista, A.M., Leen, T.K., Lu, Z. & van der Merwe, R. 2009. Fast data assimilation using a nonlinear Kalman filter and a model surrogate: An application to the Columbia River estuary. *Dynamics of Atmospheres and Oceans* 48(1-3): 16-45.

Hodskinson, A. & Ferguson, R.I. 1998. Numerical modelling of separated flow in river bends: model testing and experimental investigation of geometric controls on the extent of flow separation at the concave bank. *Hydrological Processes* 12(8): 1323-1338.

Holmes, P., Lumley, J.L. & Berkooz, G. 1998. *Turbulence, coherent structures, dynamical systems and symmetry*, Cambridge: Cambridge University Press.

Kang, S., Lightbody, A., Hill, C. & Sotiropoulos, F. 2011. High-resolution numerical simulation of turbulence in natural waterways. *Advances in Water Resources* 34(1): 98-113.

Lane, S.N., Bradbrook, K.F., Richards, K.S., Biron, P.A. & Roy, A.G. 1999. The application of computational fluid dynamics to natural river channels: three-dimensional versus two-dimensional approaches. *Geomorphology* 29(1-2): 1-20.

Lumley, J. 1967. The Structure of Inhomogeneous Turbulent Flows. In A. Yaglom & V. Tatarski (eds), *Atmospheric turbulence and radio propagation*: 166-178. Moscow: Nauka.

Ma, L., Ashworth, P.J., Best, J.L., Elliott, L., Ingham, D.B. & Whitcombe, L.J. 2002. Computational fluid dynamics and the physical modelling of an upland urban river. *Geomorphology* 44(3-4): 375-391.

Mokhasi, P., Rempfer, D. & Kandala, S. 2009. Predictive flow-field estimation. *Physica D: Nonlinear Phenomena* 238(3): 290-308.

Rodi, W. 2010. Large eddy simulation of river flows. In *Proceedings of the International Conference on Fluvial Hydraulics, River Flow 2010*: 23-32. Karlsruhe, Germany: Bundesanstalt fur Wasserbau.

Rodriguez, J.F., Bombardelli, F.A., García, M.H., Frothingham, K.M., Rhoads, B.L. & Abad, J.D. 2004. High-resolution Numerical Simulation of Flow Through a Highly Sinuous River Reach. *Water Resources Management* 18(3): 177-199.

Shimizu, Y., Yamaguchi, H. & Itakura, T. 1990. Three-dimensional computation of flow and bed deformation. *Journal of Hydraulic Engineering* 116(9): 1090–1108.

Sinha, S.K., Sotiropoulos, F. & Odgaard, A.J. 1998. Three-dimensional numerical model for flow through natural rivers. *Journal of Hydraulic Engineering* 124(1): 13–24.

Sirovich, L. & Kirby, M. 1987. Low-dimensional procedure for the characterization of human faces. *Journal of the Optical Society of America A* 4(3): 519-524.

Stacey, M.T., Monismith, S.G. & Burau, J.R. 1999. Observations of Turbulence in a Partially Stratified Estuary. *Journal of Physical Oceanography* 29(8): 1950-1970.

Warner, J.C., Geyer, W.R. & Lerczak, J.A. 2005. Numerical modeling of an estuary: A comprehensive skill assessment. *Journal of Geophysical Research* 110(C5).

Yildirim, B., Chryssostomidis, C. & Karniadakis, G.E. 2009. Efficient sensor placement for ocean measurements using low-dimensional concepts. *Ocean Modelling* 27(3-4): 160–173.